PHYSICAL REVIEW A VOLUME 47, NUMBER 6 JUNE 1993

Classical-quantum correspondence in the driven surface-state-electron model

Miroslaw Latka
Physics Department, University of North Texas, Denton, Texas 76203

Paolo Grigolini
Physics Department, University of North Texas, Denton, Texas 76203
and Instituto di Biofisica del Consiglio Nazionale delle Ricerche, Via S. Lorenzo 28, 56127 Pisa, Italy

Bruce J. West
Physics Department, University of North Texas, Denton, Texas 76203
(Received 12 November 1992)

The quantum dynamics of minimum uncertainty wave packets in a system described by the surface-state-electron Hamiltonian are studied herein. The quantum evolution is found to be strongly dependent upon the orbit structure in the classical phase space. A Gaussian wave packet, initially centered on the part of the phase space incased by Kolmogorov-Arnold-Moser tori remains localized, while the packets located in the chaotic region spread rapidly, filling the available phase space. To quantify the observed spreading quantum uncertainty is introduced as a dynamical variable, and its time development is determined by the ballistic growth of the position uncertainty and the erratic oscillations of the momentum uncertainty. The quantum evolution is analyzed within the framework of the Floquet formalism. The Floquet spectrum of the stable packet is shown to be dominated by a few quasienergy states with the corresponding Husimi distribution embedded in the classical stability island. Further, the classical concept of diffusion previously used in this context is shown to be inappropriate.

PACS number(s): 03.65.Sq, 05.45.+b

I. INTRODUCTION

The correspondence principle of Bohr, which states that the results of classical and quantum-mechanical calculations should converge in the limit of high quantum numbers or small $\hbar$, has recently become problematic with the recognition of chaotic trajectories in the classical domain. The nonintegrability of such Hamiltonian system has led to a flurry of studies of a number of simple physical models and the exploration of the analogous experimental systems. In this paper we consider the aspect of classical-quantum correspondence concerning the differences between quantum dynamics in the classically regular and classically chaotic regions of phase space. This problem was recently studied by, among others, Lin and Ballentine [1,2] and Plata and Llorente [3] for a monochromatically driven double-well potential. It was found that a Gaussian wave packet may undergo coherent or incoherent motion depending upon whether the initial position of the wave packet is in the regular or irregular part of the phase space. The Poincaré surface of section of this system has a small regular island in each well immersed in a chaotic sea which extends over both wells. It is shown numerically by Lin and Ballentine [1,2] that a wave packet initially centered on one stability island tunnels to the other one. The tunneling between the classical phase-space structures retains its coherent, oscillatory nature despite the fact that the wave packet is not completely enclosed by the Kolmogorov-Arnold-Moser (KAM) surfaces. The driven tunneling phenomenon has a rate 10^4 faster than that for the undriven case and is determined by the energy splitting of a pair of Floquet states localized on two stability regions [3]. Symmetric and antisymmetric combinations of these states yield packets initially localized in each well which in the course of time oscillate between the stability regions. On the other hand if a wave packet is launched from the classically chaotic portion of the phase space it rapidly spreads and covers the entire chaotic sea.

Lin and Ballentine [2] suggest that while localized quasienergy states (in the case of periodically perturbed systems) are associated with regular islands in the classical phase space, the extended states correspond to the chaotic sea. Consequently, if the wave packet is initially located in the regular island its time evolution will be determined by a small number of very well localized quasienergy states. Therefore the time development of the dynamical variables should appear regular. On the other hand, a packet launched from the chaotic part of the phase space is a superposition of a great number of the extended quasienergy states and produces an erratic time evolution of the dynamical variables. In the present paper we test whether this type of behavior holds for a system described by a driven surface-state-electron (SSE) Hamiltonian and may therefore be generic. The dynamics of the SSE system is quite different from that in the double-well potential mentioned above, being very complicated in both the classical and quantum domains.

The SSE model has been used to describe the ionization of highly excited hydrogenic atoms. Jensen *et al.* [4] present a quantum mechanism for the suppression of chaotic ionization that, they argue, explains the existence

of anomalously stable states observed in the microwave ionization experiments of Koch *et al.* [5]. The mechanism is the peaking of the wave function in the region of the phase space containing unstable periodic orbits; these are Heller's "scars." The scarred wave function inhibits ionization, since it remains localized in regions of phase space where the classical dynamical orbits are unstable and chaotic. They do point out, however, that we do not have a detailed understanding of the physical mechanisms that cause scarred wave functions. Herein we show that the scarred wave functions noted above may in fact be implicit in the general picture suggested by Lin and Ballentine.

The classical chaotic trajectory is herein found to assist the spreading of the quantum wave packet into the region surrounding the stable island in the classical phase space of the perturbed SSE model. This delocalization of the wave packet into the region corresponding to smaller principle quantum numbers actually stabilizes the system and inhibits ionization. The chaotic bed acts as a potential minimum into which the quantum wave packet is drawn. Thus the SSE model manifests chaos-induced stability, a property overlooked in the previous investigations, which emphasized the relation of the quantum ionization threshold to the onset of stochastic dynamics in the classical domain.

The present paper is organized as follows: In Sec. II we describe the driven SSE model and the method used to solve the time-dependent Schrödinger equation including some details of the Floquet formalism. In Sec. III we discuss the introduction of a quantum phase space using the Wigner formalism and its coarse-grained complement, the Husimi function. We also introduce the quantum uncertainty as a dynamical quantity and integrate the classical equations of motion. The growth of quantum uncertainty here replaces the "diffusive" energy increase as a diagnostic of the system dynamics. In Sec. IV we present the results of numerical quantum-mechanical calculations for three minimum uncertainty wave packets initially localized in different portions of phase space. In Sec. V the analysis of the quantum dynamics within the Floquet formalism is briefly discussed. In Sec. VI we draw some final conclusions. In particular we conclude that the quantum evolution of the system is never *diffusive* in the classical sense, i.e., it is never irreversible, and that the use of this nomenclature is confusing and should be avoided in a quantum-mechanical context.

II. SSE MODEL

The driven surface-state-electron model was first used in the classical analysis of microwave perturbations of electrons bound to the surface of liquid helium by their image charges. Jensen [6] emphasized that since the classical dynamical orbits of the SSE model can be chaotic in certain parameter regimes, the corresponding one-dimensional quantum system may be unique for the experimental investigation of the quantum manifestation of chaos. Jensen [7] also worked out the classical theory for the stochastic ionization of surface-state electrons, which he used to assist in our understanding of the experimental investigations of the ionization of Rydberg atoms by low-frequency microwave fields [8]. The latter experimental results indicated that the ionization was strongly dependent on the intensity of the oscillating electromagnetic field, but only weakly dependent on the frequency, thereby producing a quantum paradox. A proposed resolution of this paradox lay in the amplitude dependence of the nonlinear resonances which under sufficiently strong perturbation overlap, producing chaotic orbits in the classical analysis of the SSE model [7]. However, this resolution is not complete because although there is an apparent physical ionization mechanism based on the stochastic diffusion of the electrons in phase space, there is in addition a suppression of this effect due to *quantum localization* [4,9,10]. A complete review of these quantum manifestations of chaos is not appropriate here so we restrict ourselves to a brief review of relevant SSE formalism.

The driven SSE Hamiltonian has been extensively studied in connection with microwave ionization of highly excited hydrogen atoms (see Refs. [9,10] and references therein). In atomic units (a.u.) this Hamiltonian may be written as

$$H = H_0(x,p) + V(x,t) , \tag{1}$$

where

$$H_0 = \frac{p^2}{2} + \begin{cases} \infty , & x \le 0 \\ -\dfrac{1}{x} , & x > 0 , \end{cases} \tag{2}$$

and

$$V = xFg(t)\cos(\Omega t) . \tag{3}$$

F is the peak amplitude of the driving force, Ω is its frequency, and $g(t)$ is a slowly varying envelope function chosen to mimic the way in which the external perturbation is turned on.

Classically the Hamiltonian (1) describes both bounded and unbounded dynamical behavior. In the former case it may be rewritten in action-angle variables (I,Θ) [11]:

$$H(I,\Theta) = \frac{1}{2I^2} + 2I^2 Fg(t)\sin^2(\eta)\cos(\Omega t) , \tag{4}$$

where the canonical variables (x,p) can be expressed as

$$x = 2I^2\sin^2(\eta) , \tag{5}$$

$$p = \frac{1}{I}\cot(\eta) . \tag{6}$$

The auxiliary variable η determines the angle variable by means of

$$\Theta = 2\eta - \sin(2\eta) . \tag{7}$$

The unperturbed motion with constant action I_0 has the Kepler frequency $\omega = 1/I_0^3$ and the total energy $E = -1/(2I_0^2)$, which is the familiar expression for the hydrogenic energy spectrum.

To facilitate further discussion in this paragraph we choose $g(t)$ as a unit step function [alternatively, we could write this envelope function in the form $g(\Omega t)$]. In

this case Hamilton's equations of motion generated by (4) have a useful scaling property: if $I(t)$ and $\Theta(t)$ are the dynamical variables for the Hamiltonian with parameters F and Ω and the initial conditions I_0 and Θ_0, then $\Theta'(t')=\Theta(t/I_0^3)$ and $I'(t')=I(t/I_0^3)/I_0$ are the scaled variables for the Hamiltonian with the parameters

$$F'=FI_0^4 , \quad \Omega'=\Omega I_0^3 , \tag{8}$$

and the initial conditions 1 and Θ_0. Equivalently Hamiltonian (1) remains invariant under the transformation $F'=F\alpha^4$, $\Omega'=\Omega\alpha^3$, $t'=t/\alpha^3$, and $x'=x/\alpha^2$, with α being any real number.

The properties of the SSE Hamiltonian are conveniently described in terms of the scaled parameters (8) and in the quantum case the initial action I_0 is replaced by the principal quantum number n_0 of the initial state. With increasing scaled frequency Ω' the differences between classical and quantum dynamics become apparent [9]. When $\Omega' \gg 1$ the chaotic, diffusive behavior present in the classical system for a sufficiently strong perturbation (fairly well estimated by the Chirikov resonance overlapping criterion [12]) appears to be completely inhibited in the quantum domain. This phenomenon, known as quantum suppression of classical chaos, was also reported for the quantum kicked rotator [13]. The "diffusive behavior" in the quantum case may only be observed after the application of a perturbation which is much stronger than that required in the classical system.

Throughout this paper we shall put Planck's constant equal to unity and focus our discussion of the classical-quantum correspondence on the high quantum number case. The Schrödinger equation corresponding to (1) then reads

$$i\frac{\partial}{\partial t}|\psi\rangle=-\frac{1}{2}\frac{\partial^2}{\partial x^2}|\psi\rangle-\frac{1}{x}|\psi\rangle+xFg(t)\cos(\Omega t)|\psi\rangle . \tag{9}$$

There is no analytical solution to (9) and numerical methods must be used to obtain the time evolution of the wave function. In the most straightforward approach the wave function is expanded in the basis of eigenfunctions $|\phi_n\rangle$ of the unperturbed Hamiltonian (2)

$$|\psi(x,t)\rangle=\sum_n c_n(t)|\phi_n(x)\rangle e^{-i\epsilon_n t} , \tag{10}$$

where

$$|\phi_n(x)\rangle=\frac{2}{n^{5/2}}xe^{-x/n}L_{n-1}^{(1)}\left[\frac{2x}{n}\right] . \tag{11}$$

$L_{n-1}^{(1)}$ in (11) are associated Laguerre polynomials. The eigenfunctions (11) are closely related to the hydrogenic radial functions $R_{n,l}(r)$:

$$|\phi_n(x)\rangle=|R_{n,0}(x)\rangle/x , \tag{12}$$

where the Cartesian distance x replaces the radial distance r as the argument of $R_{n,l}$.

The Schrödinger equation (9) then leads to the set of coupled differential equations for the expansion coefficients $c_n(t)$:

$$i\dot{c}_n(t)=\sum_{n'} e^{i\omega_{nn'}t}Fg(t)\cos(\Omega t)x_{nn'}c_{n'}(t) , \tag{13}$$

$\omega_{nn'}=\epsilon_n-\epsilon_{n'}$, $\epsilon_n=-1/(2n^2)$, and $x_{nn'}=\langle\phi_n|\hat{x}|\phi_{n'}\rangle$. The diagonal matrix element of the $\hat{x}$ operator is found analytically to be

$$x_{nn}=\tfrac{3}{2}n^2 . \tag{14}$$

To obtain the off-diagonal matrix elements $x_{nn'}$ we employ the convenient method originally proposed by Susskind and Jensen [14], which relies on the momentum space representation of the basis function (11)

$$|\phi_n(p)\rangle=\frac{(2n/\pi)^{1/2}\exp[2in\ \mathrm{arccot}(np)]}{(1+n^2p^2)} \tag{15}$$

and the observation

$$(\epsilon_{n'}-\epsilon_n)\langle\phi_n|\hat{x}|\phi_{n'}\rangle=i\langle\phi_n|\hat{p}|\phi_{n'}\rangle . \tag{16}$$

The above formula may be obtained by computing the matrix elements of $[\hat{x},\hat{H}_0]=i\hat{p}$ between the eigenfunctions of $\hat{H}_0$. Using (15) and (16),

$$x_{nn'}=-\frac{8}{\pi}\frac{(nn')^{5/2}}{(n^2-n'^2)}\times\int_0^\infty p\frac{\sin[2n\ \mathrm{arccot}(np)-2n'\ \mathrm{arccot}(n'p)]}{(1+n^2p^2)(1+n'^2p^2)}dp . \tag{17}$$

However, expansion (10) does not take into account the excitation into the continuum and numerical tractability requires the use of a truncated basis. For the strength of the driving force considered in this paper continuum effects have been found to be negligible [10,14]. The main consequence of the use of the finite basis is the possible modification of probability when the levels close to the edge of the basis set become significantly populated. This effect may considerably distort the results of the numerical simulations. We have performed the calculations with several different sizes of the basis set (150, 200, 250) to assess how the results are influenced by the truncated basis approximation.

Both quantum and classical temporal evolutions strongly depend on the form of the envelope function $g(t)$. When the driving force is applied instantaneously [$g(t)$ is the unit step function], the periodicity of the Hamiltonian (1) may be exploited within the framework of the Floquet formalism. In this case the time evolution of the wave function is completely determined by a one-cycle unitary propagator $\hat{C}$,

$$|\psi((N+1)T)\rangle=\hat{C}|\psi(NT)\rangle , \tag{18}$$

where $T=2\pi/\Omega$. The eigenvalue problem for $\hat{C}$ may be written as

$$\hat{C}|\chi_n\rangle=e^{-iE_n}|\chi_n\rangle , \tag{19}$$

where the E_n, called quasienergies, are real and their corresponding eigenvectors are frequently called Floquet or quasienergy states (QES). To obtain the matrix represen-

tation of $\hat{C}$ in the basis of the $\hat{H}_0$ eigenfunctions, we notice that

$$\langle \phi_j|\psi(T)\rangle = \sum_k \langle \phi_j|\hat{C}|\phi_k\rangle\langle \phi_k|\psi(0)\rangle \ , \tag{20}$$

and if we choose the initial state such that

$$\langle \phi_k|\psi(0)\rangle = \delta_{k,j'} \ , \tag{21}$$

then

$$\langle \phi_j|\psi(T)\rangle = \langle \phi_j|\hat{C}|\phi_{j'}\rangle \ . \tag{22}$$

Thus the j' column of the matrix representation of $\hat{C}$ may be calculated using the initial conditions (21) and integrating the time-dependent Schrödinger equation over one period of the perturbation. We can then numerically solve the eigenvalue problem (19).

For times $t = NT$ the wave function may be written as

$$|\psi(NT)\rangle = \sum_n e^{-iE_n N}|\chi_n\rangle\langle\chi_n|\psi(0)\rangle \ . \tag{23}$$

It is apparent from (23) that only the Floquet states overlapping the initial wave function contribute to its subsequent time evolution. Moreover, when the initial state is a pure state with $c_{m_0}(0)=1$ then the amplitude $c_m(NT)$ to excite any given state $|\phi_m\rangle$ after N cycles of the perturbation is given by

$$c_m(NT) = \sum_n \langle \phi_m|\chi_n\rangle e^{-iE_n N}\langle\chi_n|\phi_{m_0}\rangle \ . \tag{24}$$

In order to induce a $|\phi_{m_0}\rangle \rightarrow |\phi_m\rangle$ transition there has to be at least one Floquet state which connects $|\phi_{m_0}\rangle$ with $|\phi_m\rangle$. Thus the degree of localization of the Floquet states affects the efficiency with which the system absorbs the external energy.

III. QUANTUM PHASE SPACE

Properties of classical dynamics are conveniently studied in a phase-space representation. The uncertainty principle precludes the direct transfer of this concept and that of distribution functions to quantum mechanics. Nonetheless the so-called quasiprobability distribution functions have proved to be extremely useful in studying the correspondence between classical and quantum mechanics. The Wigner function [15,16] is one of the most frequently used of these latter functions and for a one-dimensional system described by a wave function $|\psi\rangle$ is defined as

$$\rho_W(q,p) = \frac{1}{\pi}\int_{-\infty}^{\infty} \psi^*(q+y)\psi(q-y)e^{2ipy}dy \ , \tag{25}$$

where q and p are the canonically conjugate displacement and momentum. In this formalism every operator $\hat{A}(\hat{q},\hat{p})$ in Hilbert space is associated, via the Weyl transformation, to a function $A_W(q,p)$:

$$A_W(q,p) = \int_{-\infty}^{\infty} \psi^*\left[q+\frac{y}{2}\right]\hat{A}(\hat{q},\hat{p})\psi\left[q-\frac{y}{2}\right]e^{ipy}dy \ . \tag{26}$$

Then the expectation value of the $\hat{A}$ operator may be cast in the form similar to that used in classical mechanics:

$$\langle\psi|\hat{A}|\psi\rangle = \int_{-\infty}^{\infty}dq\int_{-\infty}^{\infty}dp\ A_W(q,p)\rho_W(q,p) \ . \tag{27}$$

The Wigner function has very interesting properties but it is not positive definite so that formally it cannot be considered to be a probability density function. It usually oscillates violently, which is especially well pronounced in the case of the SSE Hamiltonian. The Wigner distribution of the quantum system described by the eigenfunction $|\phi_n\rangle$ of $\hat{H}_0$ has an oscillatory character which becomes a serious numerical problem for principal quantum numbers as low as $n=10$ and becomes worse with increasing n. In order to faithfully display the structure of the Wigner function, one is forced to use a denser grid in the phase space with the growing principal quantum number. This is computationally inefficient although the resulting images are often quite spectacular. The Wigner function does not have a proper semiclassical limit and it was shown [17] that its time evolution differs significantly from that of an analogous classical probability distribution. To avoid these difficulties and to obtain a nonnegative distribution function with gentle undulations and the proper semiclassical limit, smoothing of the Wigner function was introduced. The Husimi function [17,18] is the simplest case of Gaussian smoothing and is defined as

$$\rho_H(q,p) = \frac{1}{\pi}\int_{-\infty}^{\infty}\int_{-\infty}^{\infty}\rho_W(q',p') \times\exp\left[-\xi(q'-q)^2-\frac{(p'-p)^2}{\xi}\right] \times dq'dp' \ , \tag{28}$$

or equivalently,

$$\rho_H(q,p) = \frac{1}{2\pi}\exp\left[\tfrac{1}{4}\left[\frac{1}{\xi}\frac{\partial^2}{\partial q^2}+\xi\frac{\partial^2}{\partial p^2}\right]\right]\rho_W(q,p) = \frac{1}{2\pi}|\langle\psi|\Phi_\alpha\rangle|^2 \ , \tag{29}$$

where

$$|\Phi_\alpha\rangle = \left[\frac{\xi}{\pi}\right]^{1/4}\exp\left[-\frac{\xi}{2}(x-q)^2+ip\left[x-\frac{q}{2}\right]\right] \tag{30}$$

is the coherent state, $\alpha=\sqrt{\xi}[q+i(p/\xi)]$, and ξ is a coarse-graining parameter. Using the expansion (10) we may rewrite (29) as

$$\rho_H(q,p,t) = \frac{1}{2\pi}\left|\sum_n c_n^*(t)\langle\phi_n|\Phi_\alpha\rangle e^{i\epsilon_n t}\right|^2 \ . \tag{31}$$

The choice of ξ is not unique and setting its value to the natural frequency of the unperturbed system was originally proposed by Husimi. However, his arguments cannot be directly employed in the present context. The choice of the coarse-graining parameter for the SSE Hamiltonian has been previously discussed [19] and is based on the following observation [20]. If $\rho_H(q,p)$ is the

Husimi representation of a wave function $|\psi\rangle$, then

$$\langle q^2\rangle_H \equiv \int\int q^2\rho_H(q,p)dq\,dp = \langle q^2\rangle + \frac{1}{2\xi} \tag{32}$$

and

$$\langle p^2\rangle_H \equiv \int\int p^2\rho_H(q,p)dq\,dp = \langle p^2\rangle + \tfrac{1}{2}\xi\ , \tag{33}$$

where $\langle q^2\rangle = \langle\psi|\hat{q}^2|\psi\rangle$, $\langle p^2\rangle = \langle\psi|\hat{p}^2|\psi\rangle$. On the other hand,

$$\langle q\rangle_H \equiv \int\int q\rho_H(q,p)dq\,dp = \langle q\rangle\ , \tag{34}$$

$$\langle p\rangle_H \equiv \int\int p\rho_H(q,p)dq\,dp = \langle p\rangle\ , \tag{35}$$

$\langle q\rangle = \langle\psi|\hat{q}|\psi\rangle$, and $\langle p\rangle = \langle\psi|\hat{p}|\psi\rangle$. It is apparent from (32)–(35) that coarse graining artificially increases quantum fluctuations. Note that the average of the Husimi operator $A_H(q,p)$ with respect to the Husimi distribution $\langle\ \rangle_H$ is identical with the average of the Wigner operator $A_W(q,p)$ with respect to the Wigner distribution $\langle\ \rangle_W$, $\langle A_H\rangle_H = \langle A_W\rangle_W = \langle A\rangle$, i.e., the quantum average of an observable is independent of the representation of the distribution function. However, the average of q^2 or any other phase-space function may change when evaluated in the Wigner and the Husimi representations separately, as indicated by (32) and (33). In order to obtain a reliable phase-space representation of $|\psi\rangle$, we require that

$$\langle q^2\rangle \gg \frac{1}{2\xi}\ ,\quad \langle p^2\rangle \gg \tfrac{1}{2}\xi \tag{36}$$

or

$$\frac{1}{2\langle q^2\rangle} \ll \xi \ll 2\langle p^2\rangle\ . \tag{37}$$

Later in this paper we show that for large principle quantum numbers the expectation value $\langle\phi_n|\hat{q}^2|\phi_n\rangle$ for the unperturbed eigenfunctions $|\phi_n\rangle$ is proportional to n^4 and the expectation value $\langle\phi_n|\hat{p}^2|\phi_n\rangle$ is proportional to $1/n^2$. Thus the criterion (37) reads

$$\frac{1}{2n^4} \ll \xi \ll \frac{2}{n^2}\ , \tag{38}$$

if we choose the coarse-graining parameter in (38) equal to the natural frequency of the state $|\phi_n\rangle$: $\xi = 1/n^3$, then this relation is satisfied. One should realize however that these arguments are valid only for a pure state. If one investigates the time evolution of a strongly perturbed system or if an initial condition is chosen as a linear combination of pure states (e.g., the minimum uncertainty wave packets considered in this paper) the situation becomes much more involved. For all the Husimi functions presented in this paper we use $\xi = 1/(66)^3$ a.u., which is the frequency of the driving force. This choice assures the faithful phase-space representation of the hydrogenic basis states without the excessive distortion of the minimum uncertainty wave packets used in the simulations.

The Husimi representation $H_H(q,p)$ of the Hamiltonian $\hat{H}(\hat{q},\hat{p})$ is defined by [17]

$$H_H(q,p) = \exp\left[\frac{1}{4}\left[\frac{1}{\xi}\frac{\partial^2}{\partial q^2} + \xi\frac{\partial^2}{\partial p^2}\right]\right] H_W(q,p)$$

$$= \langle\Phi_\alpha|\hat{H}|\Phi_\alpha\rangle\ . \tag{39}$$

The time evolution of the Husimi function may be written as [17,21,22]

$$\frac{\partial\rho_H}{\partial t} = \{H_H,\rho_H\} + \frac{\hbar}{2}\left[\frac{1}{\xi}\frac{\partial^2 H_H}{\partial q^2} - \xi\right]\frac{\partial^2\rho_H}{\partial q\,\partial p}$$

$$+ \frac{2}{\hbar}\sum_{l=3}^{\infty}\frac{\partial^l H_H}{\partial q^l}\mathrm{Im}\left\{\left[\frac{\hbar}{2}\left[\frac{1}{\xi}\frac{\partial}{\partial q} + i\frac{\partial}{\partial p}\right]\right]^l\right\}\rho_H\ , \tag{40}$$

where Planck's constant is written explicitly to distinguish between the "classical" contribution to the time development given by the Poisson bracket and the "quantum" contribution represented by the third term. Im in the above equation denotes the imaginary part of the following quantity. The second term in (40) arises from coarse graining and does not have a quantum origin.

To describe the propagation of a Gaussian wave packet we calculate the time evolution of the quantum uncertainty U using the position uncertainty ΔX and the momentum uncertainty ΔP:

$$U = \Delta X\Delta P\ , \tag{41}$$

where the position uncertainty is given by the variance

$$\Delta X(t) = [\langle\psi(t)|\hat{x}^2|\psi(t)\rangle - (\langle\psi(t)|\hat{x}|\psi(t)\rangle)^2]^{1/2}\ , \tag{42}$$

and the momentum uncertainty is given by the variance

$$\Delta P(t) = [\langle\psi(t)|\hat{p}^2|\psi(t)\rangle - (\langle\psi(t)|\hat{p}|\psi(t)\rangle)^2]^{1/2}\ . \tag{43}$$

Using expansion (10) we may write the moments in (42) and (43) generically as

$$\langle\psi(t)|\hat{O}|\psi(t)\rangle = \sum_{i,j} c_i^*(t)c_j(t)\langle\phi_i|\hat{O}|\phi_j\rangle e^{i\omega_{ij}t}\ , \tag{44}$$

where $\hat{O} = \hat{x}$, $\hat{x}^2$, $\hat{p}$, $\hat{p}^2$, etc. The above coefficients $c_i(t)$ are solutions to Eqs. (13). The nondiagonal matrix elements of the $\hat{x}$ operator are given by (17) and employing (16) we obtain the nondiagonal matrix elements for the $\hat{p}$ operator:

$$p_{nn'} = \langle\phi_n|\hat{p}|\phi_{n'}\rangle = ix_{nn'}(\epsilon_n - \epsilon_{n'})\ , \tag{45}$$

while

$$p_{nn} = 0\ . \tag{46}$$

The calculation of the matrix elements for $\hat{x}^2$ and $\hat{p}^2$ may be efficiently performed in the momentum space repre-

sentation; using (15) we obtain

$$p^2_{nn'}=\frac{4\sqrt{nn'}}{\pi} \times \int_0^\infty \frac{p^2\cos[2n\ \mathrm{arccot}(np)-2n'\ \mathrm{arccot}(n'p)]}{(1+n^2p^2)(1+n'^2p^2)}dp\ , \tag{47}$$

$$p^2_{nn}=\frac{1}{n^2}\ . \tag{48}$$

To evaluate the matrix elements of $\hat{x}^2$ we additionally employ its momentum space representation $-(\partial^2/\partial p^2)$ to arrive at

$$x^2_{nn'}=-\frac{8n'^2\sqrt{nn'}}{\pi}\int_0^\infty \frac{(3n'^2p^2-2n'^2-1)\cos(f)-6n'^2p\sin(f)}{(1+n'^2p^2)^3(1+n^2p^2)}dp\ , \tag{49}$$

$f=2n'\ \mathrm{arccot}(n'p)-2n\ \mathrm{arccot}(np)$,

$$x^2_{nn}=\frac{n^2(1+5n^2)}{2}\ . \tag{50}$$

Using (14), (46), (48), and (50) we derive the following formula for the position uncertainty ΔX_n, the momentum uncertainty ΔP_n, and the total uncertainty U_n of the eigenstate $|\phi_n\rangle$ of the unperturbed Hamiltonian $\hat{H}_0$:

$$\Delta X_n=n(\tfrac{1}{2}+\tfrac{1}{4}n^2)^{1/2}\ , \tag{51}$$

$$\Delta P_n=\frac{1}{n}\ , \tag{52}$$

$$U_n=(\tfrac{1}{2}+\tfrac{1}{4}n^2)^{1/2}\ . \tag{53}$$

Equations (51) and (52) have a very simple interpretation in the pseudoprobability phase space [19]. With the growing principal quantum number n the Husimi representation of $|\phi_n\rangle$ is stretched along the position axis and contracted along the momentum axis which reflects the structure of the corresponding classical trajectory. Moreover, the maximum of the distribution is peaked at the turning point $2n^2$ of the classical trajectory. From Eq. (53) we can see that for large n the quantum uncertainty grows approximately linearly with n. The integrals in (17), (47), and (49) have been calculated numerically and in some cases tested against the analytical results obtained with the help of the symbolic algebra packages (e.g., MATHEMATICA).

The singularity of the Hamiltonian (1) at $x=0$ causes problems during numerical integration of the classical equations of motion. To circumvent these difficulties we used the regularization method suggested by Leopold and Richards [23]. It is based upon the use of the extended phase space in which time and energy are considered as two additional conjugate variables. In this way the theory of canonical transitions may be extended to include time [24] since it is one of the generalized coordinates. In the case of the driven SSE Hamiltonian the extended phase space is four-dimensional (x,p,t,p_2) with $p_2=-H(x,p,t)$ being a generalized momentum conjugated to t. We introduce the new Hamiltonian given by

$$\Gamma^*=p_2+H(x,p,t)\ , \tag{54}$$

which is by definition identically equal to zero. If we parametrize the trajectories in the extended phase by t^* one of the Hamilton's equations of motion reads

$$\frac{dt}{dt^*}=\frac{\partial}{\partial p_2}\Gamma^*=1 \tag{55}$$

or

$$t=t^*+\mathrm{const}\ . \tag{56}$$

The remaining equations are the same as in standard Hamiltonian theory. In this formalism time transformation is accomplished by multiplying Γ^* by an arbitrary function. In order to remove the singularity at $x=0$ the new Hamiltonian may be formed:

$$\Gamma=4x\Gamma^*=4xp_2+2xp^2+4Fg(t)x^2\cos(\Omega t)-4\ . \tag{57}$$

The canonical transformations

$$x=q_1^2\ ,\quad p_1=2q_1p \tag{58}$$

and the change of notation $t\rightarrow q_2$, $\Gamma+4\rightarrow\Gamma$ enables one to write (57) as

$$\Gamma=\tfrac{1}{2}p_1^2+4p_2q_1^2+4Fg(q_2)q_1^4\cos(\Omega q_2)\ . \tag{59}$$

When $g(t)$ is chosen as a unit step function then the Hamiltonian Γ yields the following equations of motion:

$$\dot{q}_1=\frac{\partial\Gamma}{\partial p_1}=p_1\ , \tag{60}$$

$$\dot{p}_1=-\frac{\partial\Gamma}{\partial q_1}=-8q_1p_2-16Fq_1^3\cos(\Omega q_2)\ , \tag{61}$$

$$\dot{q}_2=\frac{\partial\Gamma}{\partial p_2}=4q_1^2\ , \tag{62}$$

$$\dot{p}_2=-\frac{\partial\Gamma}{\partial q_2}=4F\Omega q_1^4\sin(\Omega q_2)\ . \tag{63}$$

To optimize the numerical calculations the set of equations (60)–(63) was integrated in the vicinity of the singularity and the standard Hamiltonian equations of motion were used elsewhere.

IV. NUMERICAL RESULTS

In this section we discuss the influence of the initial localization of a Gaussian wave packet in the quantum phase space on its subsequent time evolution. For all classical and quantum simulations discussed here the perturbation was turned on suddenly [$g(t)$ is a unit step function], $\Omega=1/(66)^3$ a.u. and for most of the calcula-

tions $F=0.03/(66)^4$ a.u.

In Fig. 1(a) the Poincaré surface of section of the classical phase space for $F=0.01/(66)^4$ a.u. is shown. This picture was constructed using the trajectories originating from the turning points of the classical unperturbed orbits: $q_n=2n^2$, $p_n=0$, and n is an integer selected from the interval [60,80]. For every trajectory a point was plotted in the phase space ever period T of the perturbation for a total of 200 periods. We have chosen these particular initial conditions to elucidate the structure of the nonlinear resonance corresponding to the scaled frequency $\Omega'\approx 1$. We can see from Fig. 1(a) and the blowup of the central section in Fig. 1(b), that all the trajectories are apparently stable KAM tori. Increasing the field strength to $F=0.03/(66)^4$ a.u. induces an instability in the orbits resulting in the outermost KAM tori dissolving into a chaotic sea, and the more central tori retaining their stability, cf. Fig. 2(a). The stable region of Fig. 2(a) is enhanced in Fig. 2(b), where we see that a number of the inner tori have bifurcated into sequences of stable island chains.

In further discussion we call this central region the stability island or stability region. In our quantum-mechanical calculations we use three minimum uncertainty wave packets initially localized in the phase space at $q_1=8000$ a.u., $p_1=0$; $q_2=10\,000$ a.u., $p_2=0$; and $q_3=12\,000$ a.u., $p_3=0$. We refer to these packets as P_1, P_2, and P_3, respectively. The initial Husimi functions for these three packets differ only by their location in phase space so that in Fig. 3 we present only the one corresponding to the packet P_1. The comparison of Fig. 3 with the structure of the classical phase space in Fig. 2(b) (the vertical gridlines in this picture refer to the initial position localization of the packets) shows that the packet P_1 is well embedded in the stability island while the packet P_2 just barely overlaps with the island. On the other hand, the packet P_3 is totally outside the stability region, in the chaotic portion of the phase space. The projection of the packets P_1, P_2, and P_3 on the basis state $|\phi_n\rangle$ of the unperturbed Hamiltonian is given in Fig. 4. In Figs. 5–7 we present the time evolution of these wave packets in the Husimi representation. The range of position q (0, 20 000 a.u.) and momentum p (-0.03 a.u., 0.03 a.u.) used in the presented pictures comprises only a small portion of the phase space. We have already mentioned that the Husimi distribution of the pure state $|\phi_n\rangle$ peaks in the phase space at $2n^2$. Thus the maximum value of position 20 000 a.u. corresponds to the maximum of the Husimi distribution for $n=100$. We can see from Fig. 4 that the basis expansion of the packets P_1,P_2, and

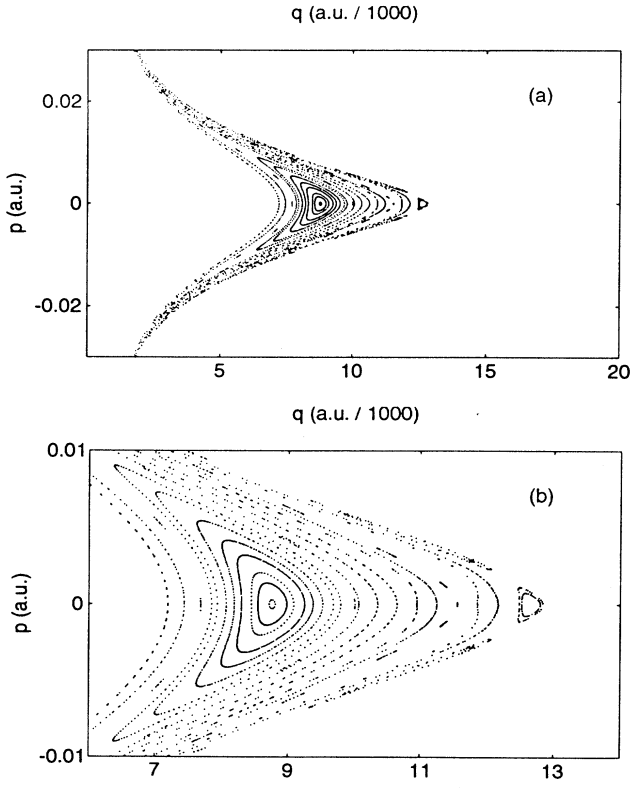

FIG. 1. (a) Poincaré surface of section for $\Omega=1/(66)^3$ a.u. and $F=0.01/(66)^4$ a.u. (b) Magnified central part of Fig. 1(a).

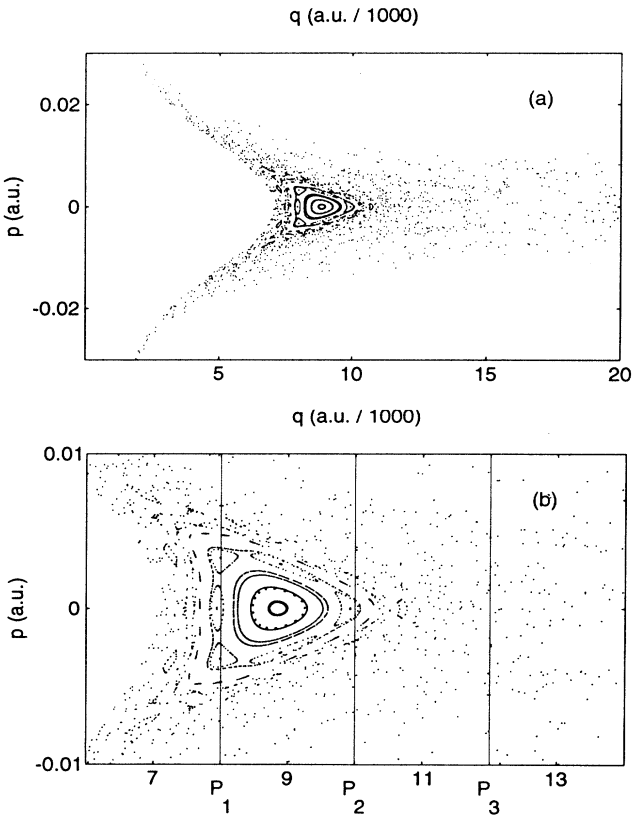

FIG. 2. (a) Poincaré surface of section for $\Omega=1/(66)^3$ a.u. and $F=0.03/(66)^4$ a.u. (b) Regular part of the classical phase space is enlarged to reveal the structure of nonlinear resonances. The vertical gridlines correspond to the position localization of three minimum uncertainty wave packets used in quantum-mechanical calculations. The packet P_1 was initially localized at $q_1=8000$ a.u., the packet P_2 at $q_2=10\,000$ a.u., and P_3 at $q_3=12\,000$ a.u.

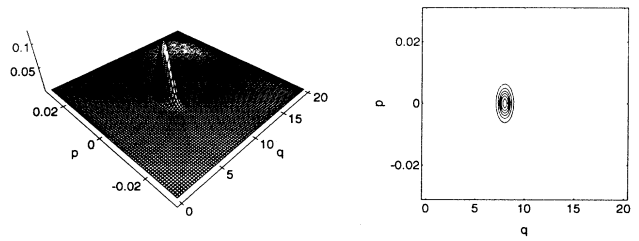

FIG. 3. Husimi function of the packet P_1 at $t=0$.

P_3 are peaked at $n_1=64$, $n_2=72$, and $n_3=79$, respectively. In the course of time the distribution function of the strongly perturbed packets may spread outside the indicated region of phase space which can be clearly seen as bumps at the edges of the pictures. The scales for the value of the Husimi distribution were chosen for maximum resolutions and usually differ from one picture to the other. In the accompanying contour plots six contour lines, uniformly spaced between zero and the maximum value of the Husimi function, were used. It should be noticed that the Husimi distributions were calculated at times which correspond to the maximum strength of the driving force so that the pictures are usually not symmetric with respect to the p axis. This is distinct from the results presented by Stevens and Sundaram [19], who investigated the time evolution of the distribution function for the SSE Hamiltonian initially prepared in a pure state; cf. (11). The symmetry of all their depicted Husimi functions with respect to momentum suggests that the expectation value $\langle \psi(t)|\hat{p}|\psi(t)\rangle$ would be identically equal to zero. Inspection of equations (44) and (45), however, as well as our numerical calculations, contradict this conjecture.

Figures 5–7 reveal a significant influence of the structure of the classical phase space on the quantum dynamics. The packet P_1 depicted in Fig. 5, originally located within the stability island, remains very well localized even after 100 cycles of the driving force, cf. Figs. 5(a)–5(c). The packets P_2 and P_3, on the other hand, undergo complicated evolution as shown in Figs. 6 and 7. It is clear that they spread out to cover the region of the phase space occupied by the outermost classical trajectories. This spreading is particularly rapid and persistent for the packet P_3. However, the time scale of the motion is short so that the presented snapshots cannot fully describe the nature of the quantum dynamics. This is demonstrated more clearly by the time evolution of the *autocorrelation function* or *survival probability*

$$S(t)=|\langle \psi(t)|\psi(0)\rangle|^2 \tag{64}$$

given in Fig. 8. Only values for times equal to multiples of the period T are plotted.

The packet P_1 in Fig. 8(a) exhibits a very interesting kind of fast collapse and revival whose amplitudes are slowly varying functions of time. The envelope of the revivals begins to decrease immediately after the perturbation is switched on. The minimal value of 0.53 occurs at $t=60T$. From the moment revivals become stronger and stronger and at $t=141T$ the survival probability achieves the value 0.92. On the other hand, the minimum of the envelope of the collapses drops to 0.02 at $t=3T$ and steadily grows to the maximum of 0.22 observed at

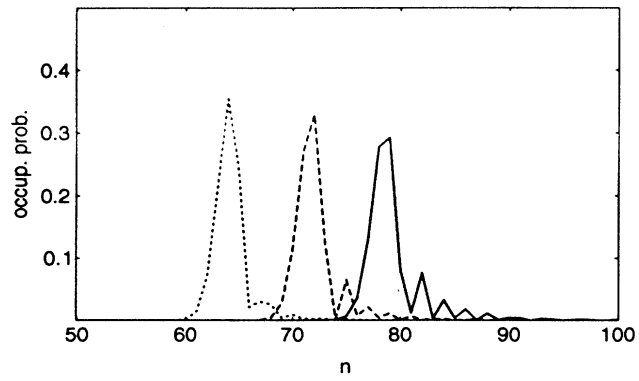

FIG. 4. Projection of three minimum uncertainty wave packets on the basis states of the unperturbed Hamiltonian $\hat{H}_0$. Dotted line corresponds to the packet P_1, dashed line to the packet P_2, and solid line to P_3.

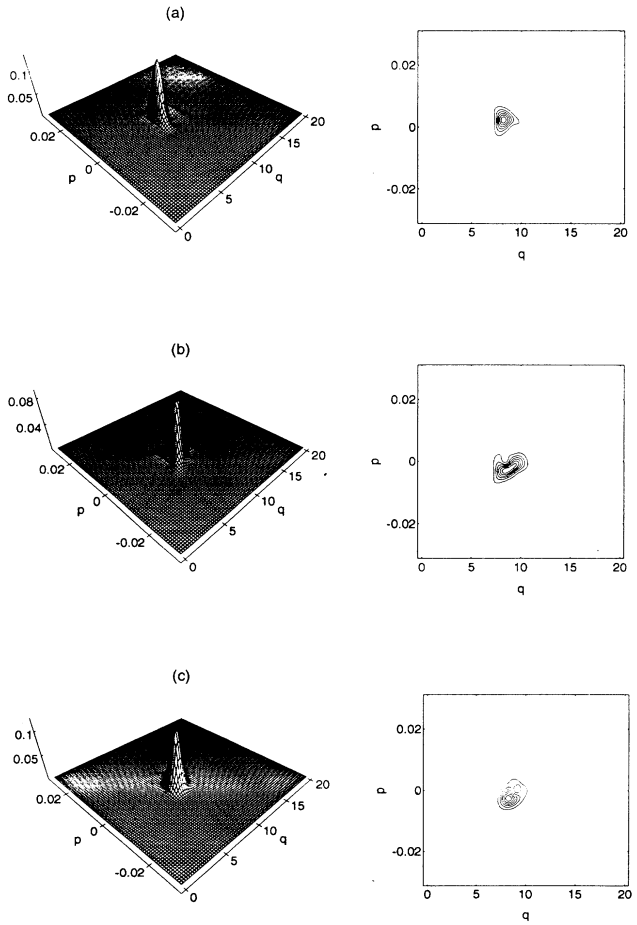

FIG. 5. Time evolution of the wave packet P_1 initially localized at the regular part of the classical phase space. The times plotted are (a) $5T$, (b) $20T$, and (c) $100T$.

$t=70T$. Then it decays gradually so that at $t=132T$ it is equal again to 0.02. The autocorrelation function is frequently used to extract information about the coherence of the quantum dynamics. The very low envelope of collapses at the early stage of the time evolution of the packet P_1 is somewhat surprising since there is very little spreading apparent in Fig. 5. The resolution of this problem is provided in Fig. 9(a) where the Husimi function for the packet P_1 at $t=3T$ is shown. The extremely low value of the autocorrelation function is primarily a result of the coherent displacement of the packet from its initial position. Another example of this type of behavior is given in Fig. 9(b) which shows the distribution function for the packet P_2 at $t=2T$ when the survival probability is equal to 0.01. In this case besides the coherent displacement a noticeable amount of spreading may also be observed. While the time development of the survival probability of the packet P_1 is quite regular the other packets P_2 and P_3 quickly lose the correlation with the initial state and their subsequent evolution seems to be erratic [cf. Figs. 8(b) and 8(c)]. Despite this irregular behavior the autocorrelation function may be as high as 0.44 at $t=16T$ for the packet P_2 and 0.42 at $t=81T$ for the packet P_3, which demonstrates the presence of strong quantum-mechanical correlations. Analyzing Fig. 8(b) we discover in the initial evolution and later at $t=100T$ the ghost of the quasiperiodic behavior of the packet P_2. There is no similar behavior in Fig. 8(c) which corresponds to the packet P_3. This observation provides additional evidence that the quantum dynamics is strongly affected by the structure of the classical trajectories in phase space.

A quantitative measure of the spreading observed in the above pictures is given by the quantum uncertainty [cf. (41)–(44)]. In Fig. 10 the change in $U(t)$ over time is graphed for P_1, P_2, and P_3. It is clear from this figure that there is essentially no change from the initial uncertainty in P_1, that the uncertainty in P_2 is substantially larger, and that in P_3 is the greatest of the three. If we examine the position uncertainty and momentum uncertainty separately in Figs. 11 and 12 we can see that the large oscillations in $U(t)$ are primarily due to abrupt changes in the momentum uncertainty over time. The character of the temporal evolution of momentum uncertainty may be elucidated if one realizes that the minimum uncertainty wave packet is the linear combination of

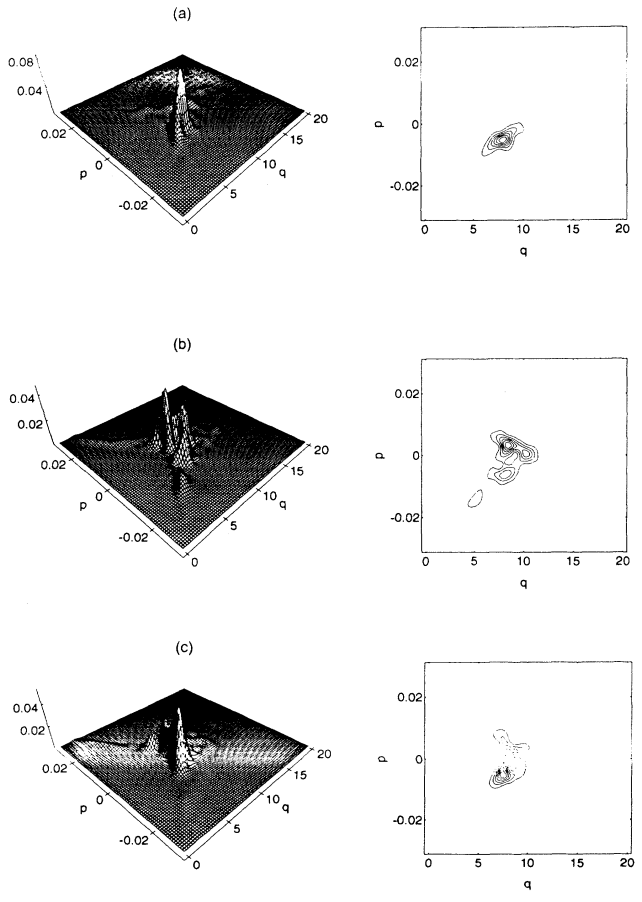

FIG. 6. Time evolution of the wave packet P_2 initially overlapping with the regular part of the classical phase space. The times plotted are (a) $5T$, (b) $20T$, and (c) $100T$.

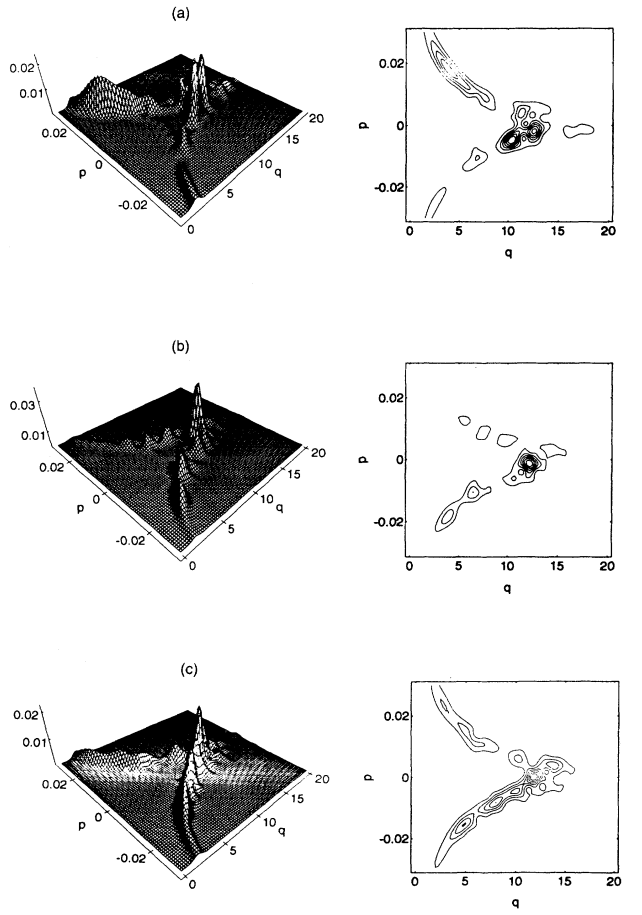

FIG. 7. Time evolution of the wave packet P_3 initially localized in the chaotic region of the classical phase space. The times plotted are (a) $5T$, (b) $20T$, and (c) $100T$.

many unperturbed basis states, each having a different natural frequency. The superposition of motions with the different frequencies yields the observed erratic behavior. This interpretation was confirmed in our numerical calculations performed on the driven SSE Hamiltonian initially prepared in the state $|\phi_{n_0}\rangle$. If the external perturbations are strong enough to significantly populate several basis states the momentum uncertainty exhibits irregular evolution. Otherwise it is a slowly varying function of time. There is some short-time variation in the position uncertainty, but its time evolution is dominated by an *apparent diffusion process.* If we disregard the transient, the position uncertainty of P_2 and P_3 grows *ballis-*

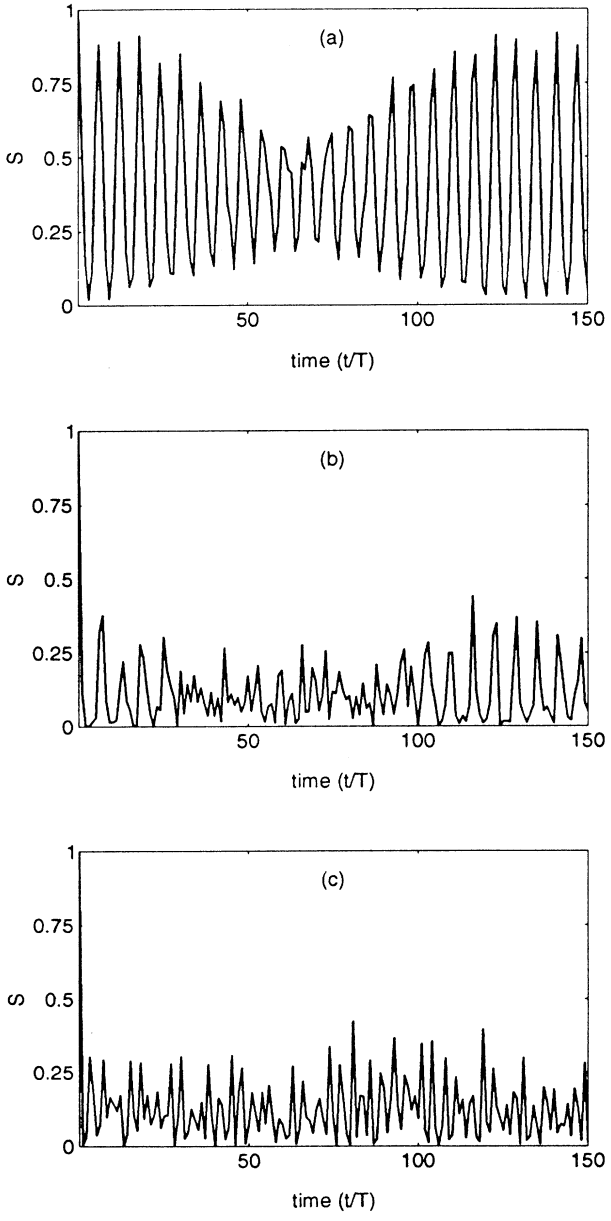

FIG. 8. Survival probability $S(t)=|\langle\psi(t)|\psi(0)\rangle|^2$ for (a) wave packet P_1, (b) wave packet P_2, and (c) wave packet P_3.

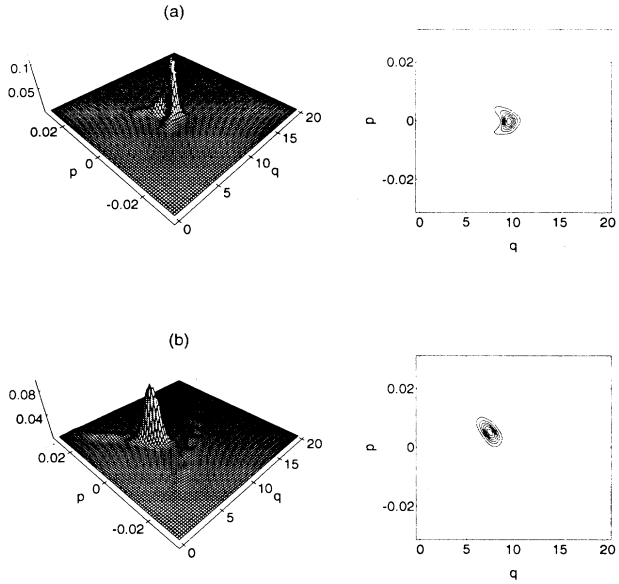

FIG. 9. Husimi function of (a) the packet P_1 at $t=3T$, (b) the packet P_2 at $2T$.

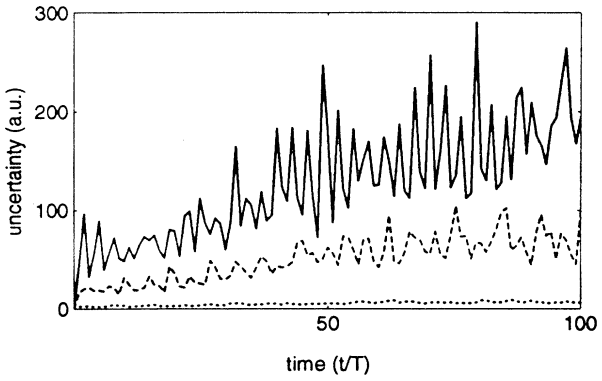

FIG. 10. Time evolution of quantum-mechanical uncertainty. Dotted line corresponds to the packet P_1, dashed line to the packet P_2, and the solid line to the packet P_3.

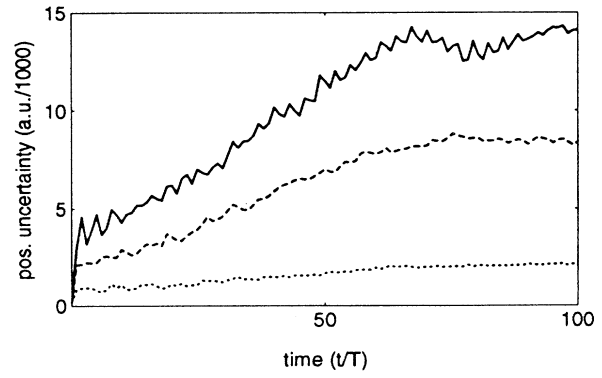

FIG. 11. Time evolution of position uncertainty. The legend same as in Fig. 10.

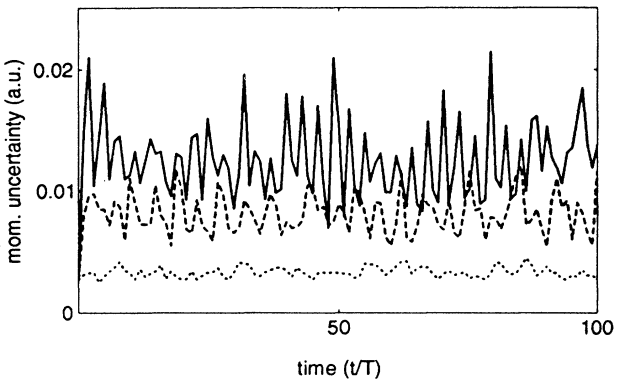

FIG. 12. Time evolution of momentum uncertainty. The legend same as in Fig. 10.

tically with time $\Delta X \propto t$. Note that this is *not* the diffusive mechanism discussed by Casati *et al.* [9] and later by Jensen, Susskind, and Sanders [10]. They discussed the diffusion of action in action-angle space using a Fokker-Planck equation with an action-dependent diffusion coefficient. Here the "diffusion" is in configuration space.

Finally we may attempt to draw the conclusion that the quantum dynamics may be stabilized in the vicinity of the regular regions in the classical phase space. This behavior was also found in the driven double-well oscillator [1] and in the case of the SSE Hamiltonian prepared in the pure state $|\phi_{n_0}\rangle$ discussed earlier by Jensen *et al.* [4]. However, both Lin and Ballentine [1,2] and Takahashi and Saito [25,26] found that if the wave packet is located in a classically chaotic region it spreads to cover the entire chaotic sea. The comparison of the Husimi functions shown in Fig. 7 with the structure of the classical phase space Fig. 2 suggests that this scenario is also applicable to the perturbed SSE Hamiltonian. We should realize however that the time evolution of the Husimi function is the intricate interplay of "classical" and "quantum" terms in Eq. (40). This interplay was discussed by Bonci *et al.* [27,28] with regard to the evolution of the Wigner distribution in their discussion of a two-level atomic system interacting with a one-mode radiation field. As a result of this interplay the portion of the phase space accessible to the quantum wave packet is in the present study sharply reduced compared to the classical trajectories. Moreover, despite the spreading the wave packet retains its quantum properties as is clearly reflected in the time development of the survival probability. The presence of quantum interference is also manifested in the structure of the Husimi distribution which does not uniformly cover the phase space but is usually made up of several "islands."

V. FLOQUET ANALYSIS

The importance of Floquet theory goes beyond the numerical efficiency which becomes significant only when the number of periods of integration is much larger than the number of basis states. There is general consensus [29] about the functional form of the distribution of nearest-neighbor quasienergy level spacing. When the corresponding classical system undergoes a transition from integrable motion to chaotic motion it is reflected in the change of level statistics from Poisson-like to Wigner-like (avoided level crossing distribution). Moreover, it was shown by Graffi, Paul, and Silverstone [30] that the threshold for avoided level crossing coincides with that predicted by Chirikov's resonance criterion [12] for the onset of stochastic behavior in classical Hamiltonian systems.

The Floquet approach was used to estimate the threshold for the onset of ionization in the SSE Hamiltonian [11,31–33]. For small perturbations the Floquet eigenvectors overlapping the initial wave packet are well localized about the unperturbed hydrogen eigenfunctions. When the strength of the perturbation exceeds a critical value, quasienergy vectors spread out which via Eq. (24)

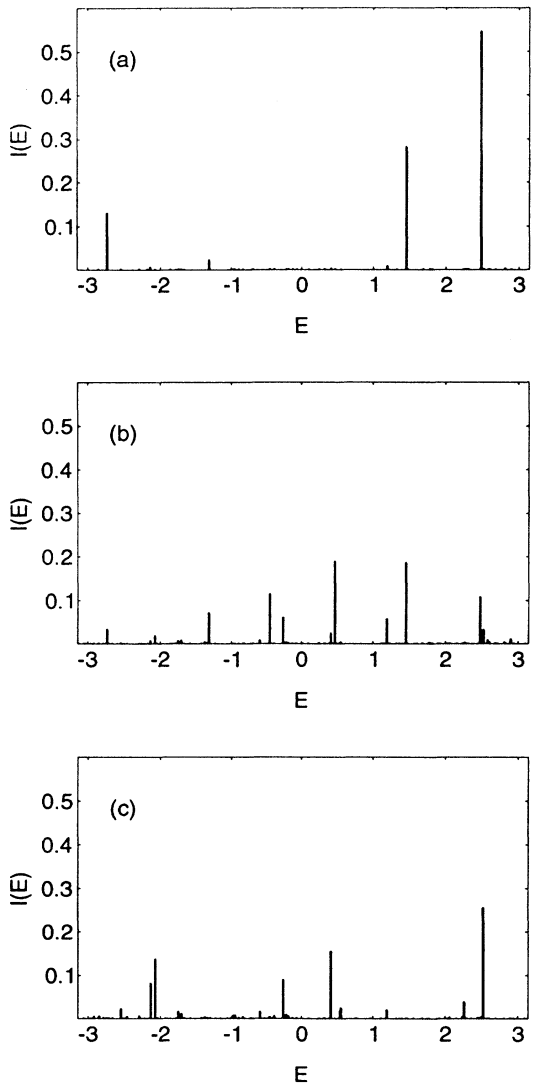

FIG. 13. Floquet spectra corresponding to the wave packets (a) P_1, (b) P_2, and (c) P_3.

lead to a rapid delocalization of the initial wave packet. Jensen *et al.* [4] have shown that the kind of Husimi representation of quasienergy states excited at the end of the slow switch-on of the perturbation are highly localized near unstable periodic orbits in the chaotic classical phase space. It was suggested that this provides an explanation for the existence of the anomalously stable states found in the experiments with microwave-perturbed highly excited hydrogen atoms. This is reminiscent of the scarred wave functions found by Heller [34] in the stadium billiard or the wave function of the Rydberg atom in a strong magnetic field [35].

We have already pointed out (23) that only Floquet states initially overlapping the wave function contribute to its time development. We define the Floquet spectrum as [3]

$$I(E)=\sum_i |\langle \psi(0)|\chi_i\rangle|^2 \delta(E-E_i) \ . \tag{65}$$

$I(E)$ is given in Fig. 13 for the three cases studied. The spectrum of P_1 as shown in Fig. 13(a) is dominated by two QES, $E_1=2.477$ with $I_{P_1}(E_1)=0.546$ and $E_2=1.452$ with $I_{P_2}(E_2)=0.281$. The Husimi representations of these states are shown in Fig. 14. We can see from this picture that both states are very well localized. The total uncertainty is equal to $\Delta U_{E_1}=4.1$ a.u. for the state E_1 and $\Delta U_{E_2}=3.6$ a.u. for the state E_2. These values of the quantum uncertainty are very low in comparison with the uncertainty of the eigenfunctions $|\phi_n\rangle$ peaked in the same region of the phase space. Calculating (53) for $n=66$ we obtain the uncertainty of 33 a.u. Moreover, the comparison with the portrait of the classical phase space Fig. 2(b) shows that these Floquet states are embedded in the stability island. While the dynamics

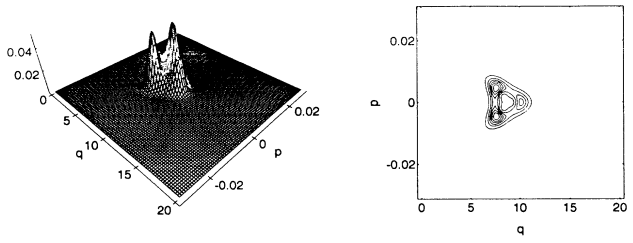

FIG. 15. Husimi representation of the quasienergy state significantly overlapping with the packet P_2: $E_3=0.476$, $I_{P_2}(E_3)=0.189$. This packet overlaps also with the QES from Fig. 14(b), in this case $I_{P_2}(E_2)=0.185$.

of P_1 is determined by a very small number of QES, the time evolution of P_2 and P_3 involves a great number of them. Figure 15 shows the Husimi distribution of the QES $E_3=0.476$ [cf. Fig. 13(c)] with the largest overlap with the packet P_2, $I_{P_2}(E_3)=0.189$. The total uncertainty of this state is $\Delta U_{E_3}=4.7$ a.u. It happens that the Floquet state from Fig. 14(b) also significantly overlaps with the packet P_2, $I_{P_2}(E_2)=0.185$. The Husimi representations of two Floquet states from the spectrum of P_3, $E_4=2.522$ with $I_{P_3}(E_4)=0.255$ and $E_5=0.415$ with $I_{P_3}(E_5)=0.155$ are presented in Fig. 16. The spatial extension of the distribution functions from Fig. 16 is much greater than those from Figs. 14 and 15. This is clearly reflected in the total uncertainty which for the state E_4 is equal to $\Delta U_{E_4}=79.3$ a.u. and for E_5 is equal to $\Delta U_{E_5}=77.8$ a.u. The significant difference between the QES from the spectrum of the packet P_3 and those from the spectrum of P_2 becomes apparent when we compare

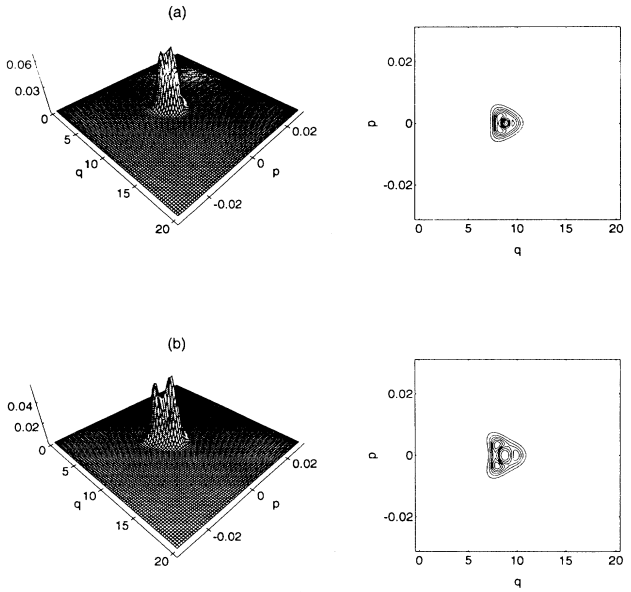

FIG. 14. Husimi representation of two quasienergy states significantly overlapping with the packet P_1: (a) $E_1=2.477$, $I_{P_1}(E_1)=0.546$, (b) $E_2=1.452$, $I_{P_1}(E_2)=0.281$.

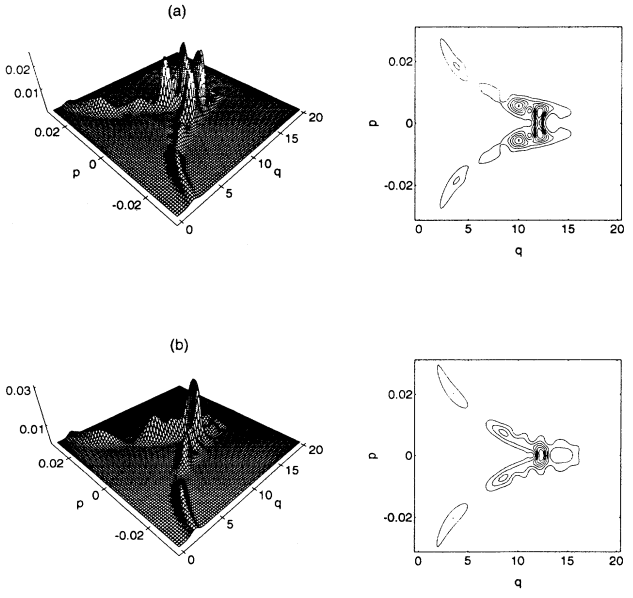

FIG. 16. Husimi representation of two quasienergy states significantly overlapping with the packet P_3: (a) $E_4=2.522$, $I_{P_3}(E_4)=0.255$. (b) $E_5=0.415$, $I_{P_3}(E_5)=0.155$.

the values of the total uncertainty for five dominant Floquet states from Figs. 13(b) and 13(c). For the packet P_2 the uncertainty varies from 4.1 to 11.6 a.u., while for the packet P_3 it varies from 27.1 to 84.2 a.u. We would like to stress another feature of the Husimi functions in Fig. 16, namely, the long tails mimicking the structure of the classical trajectories. This observation may be used as a heuristic explanation of the migration of the packet P_3 into the region of the phase space corresponding to low quantum numbers.

We conclude this section with a brief discussion of the general properties of the quasienergy states of the SSE Hamiltonian. Bardsley *et al.* [32] classified the Floquet states into three groups on the basis of their expansion over the eigenfunctions $|\phi_n\rangle$: (i) state which primarily overlap with a single low n state and thus do not differ significantly from $|\phi_n\rangle$, (ii) transitional states, and (iii) states which mainly overlap with high n states and whose expansion coefficients decay as a power of n for large n.

Type (i) and (ii) states are always present in the spectrum of the Floquet operator $\hat{C}$. The range of the transitional states depends upon the strength of the perturbation. The spectrum of the packets P_1 and P_2 is composed of the very well localized transitional states with low values of the quantum uncertainty. We have found the distribution functions of the most localized states to be centered over the classical stability island [cf. Fig. 14], which shows the way in which the structure of the Floquet states reflects the properties of the classical phase space.

VI. CONCLUSIONS

In this paper we have investigated the influence of the structure of the classical phase space on the quantum dynamics of certain minimum uncertainty wave packets. We have found that the packets initially overlapping the regular regions of phase space remain localized, while the packets centered on the classical chaotic sea spread rapidly. We analyzed the quantum dynamics using the Floquet formalism and determined that the Floquet spectrum of the stable packets is dominated by a few quasienergy states whose Husimi distributions are very well localized in the classical stability islands. Moreover, we have found that the most localized Floquet states are peaked in the vicinity of the stable island. The spectrum of the most unstable wave packet is made up of the greatest number of the QES whose corresponding distribution functions are usually very elongated, thereby mimicking the shape of classical trajectories To elucidate the complicated nature of the quantum evolution we introduced the quantum uncertainty as a dynamical variable. In the presence of the spreading of the wave packet the time development of its quantum uncertainty is determined by the monotonic growth of position uncertainty and the erratic oscillations of the momentum uncertainty. Surprisingly enough, the position uncertainty increases ballistically with time $\Delta X \propto t$ until the packet fills the available portion of the phase space. We stress that apart from significant spreading the quantum interference effects are clearly pronounced both in the time evolution of the survival probability and in the structure of the Husimi distributions. To emphasize the quantum nature of these results we performed a "time-reversal" experiment, reversing the direction of the time evolution at the point when the spreading of the wave packets was almost completed. As far as the numerical calculations are concerned the time reversal may be accomplished either by changing the direction of time during the numerical integration of the set of equations (13) or while using the Floquet method by replacing the evolution operator $\hat{C}$ by the adjoint operator $\hat{C}^{\dagger}$. In Fig. 17 we see that at $t=50T$, the point at which the evolution was reversed, the position uncertainty of the packet P_3 retraces its path as shown by the symmetry of the curve. This reversibility is a clear manifestation of quantum coherence throughout the "diffusion" of this packet. In the same way the corresponding correlation function (survival probability) depicted in Fig. 18 denotes the time reversibility of the evolution process. Thus we see that the term diffusion is misleading in this context and ought to be abandoned.

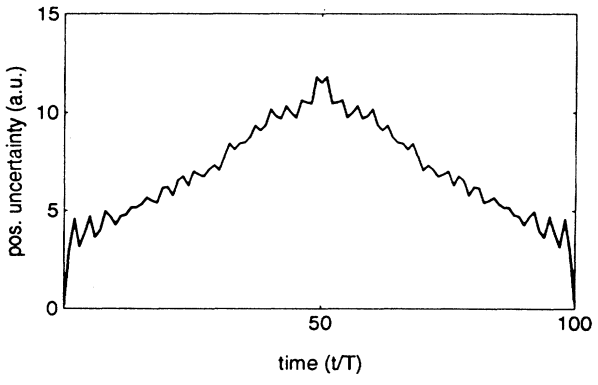

FIG. 17. Time reversal experiment for the position uncertainty for the packet P_3. At $t=50T$ the time evolution was reversed. The symmetry of the curve shows the reversibility of the quantum dynamics.

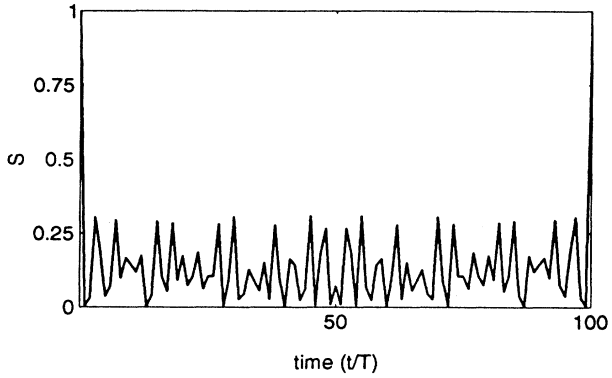

FIG. 18. Survival probability for the time-reversal experiment from Fig. 17.

ACKNOWLEDGMENTS

The authors acknowledge the partial support of this research by the Texas Advanced Research Program (Project No. 0035494-038) and thank the National Science Foundation for support of the numerical calculations performed on the CRAY Y-MP at the Pittsburgh Supercomputing Center (Grant No. PHY920023P).

[1] W. A. Lin and L. E. Ballentine, Phys. Rev. Lett. **65**, 2927 (1990).
[2] W. A. Lin and L. E. Ballentine, Phys. Rev. A **45**, 3637 (1992).
[3] J. Plata and J. M. Gomez Llorente, J. Phys. A **25**, L303 (1992).
[4] R. V. Jensen, M. M. Sanders, M. Saraceno, and B. Sundaram, Phys. Rev. Lett. **63**, 2771 (1989).
[5] P. M. Koch, in *Chaos: Proceedings of a Soviet-American Conference,* edited by D. K. Campbell (AIP, New York, 1990).
[6] R. V. Jensen, Phys. Rev. Lett. **49**, 1365 (1982).
[7] R. V. Jensen, Phys. Rev. A **30**, 386 (1984).
[8] J. E. Bayfield and P. M. Koch, Phys. Rev. Lett. **33**, 258 (1978); J. E. Bayfield, L. D. Gardner, and P. M. Koch, *ibid.* **39**, 76 (1977); P. M. Koch, J. Phys. (Paris) Colloq. **43**, C2-187 (1982).
[9] G. Casati, B. B. Chirikov, D. L. Shepelyansky, and I. Guarneri, Phys. Rep. **154**, 77 (1987).
[10] R. V. Jensen, S. M. Susskind, and M. M. Sanders, Phys. Rep. **201**, 1 (1991).
[11] R. Blümel and U. Smilansky, Z. Phys. D **6**, 83 (1987).
[12] B. Chirikov, Phys. Rep. **52**, 263 (1979).
[13] F. M. Izrailev, Phys. Rep. **196**, 229 (1990).
[14] S. M. Susskind and R. V. Jensen, Phys. Rev. A **38**, 711 (1988).
[15] E. P. Wigner, Phys. Rev. **40**, 749 (1932).
[16] H. Hillery, R. F. O'Connell, M. O. Scully, and E. P. Wigner, Phys. Rep. **106**, 122 (1984).
[17] K. Takahashi, Prog. Theor. Phys. Supp. **98**, 109 (1989).
[18] K. Husimi, Proc. Phys. Math. Soc. Jpn. **22**, 264 (1946).
[19] M. J. Stevens and B. Sundaram, Phys. Rev. A **39**, 2862 (1989).
[20] A. K. Rajagopal, Phys. Rev. A **27**, 558 (1983).
[21] R. F. O'Connell and E. P. Wigner, Physica **85A**, 121 (1981).
[22] R. F. O'Connell, Lipo Wang, and H. A. Williams, Phys. Rev. A **30**, 2187 (1984).
[23] J. G. Leopold and D. Richards, J. Phys. B **18**, 3369 (1985).
[24] V. Szebehely, *Theory of Orbits* (Academic, New York, 1967).
[25] K. Takahashi and N. Saito, Phys. Rev. Lett. **55**, 645 (1985).
[26] K. Takahashi, J. Phys. Soc. Jpn. **55**, 1443 (1986).
[27] L. Bonci, R. Roncaglia, B. J. West, and P. Grigolini, Phys. Rev. Lett. **67**, 2593 (1990).
[28] L. Bonci, R. Roncaglia, B. J. West, and P. Grigolini, Phys. Rev. A **45**, 8490 (1991).
[29] L. E. Reichl, *The Transition to Chaos* (Springer-Verlag, New York, 1991).
[30] S. Graffi, T. Paul, and H. J. Silverstone, Phys. Rev. A **37**, 2214 (1988).
[31] J. N. Bardsley and B. Sundaram, Phys. Rev. A **32**, 689 (1985).
[32] J. N. Bardsley, B. Sundaram, L. A. Pinnaduwage, and J. E. Bayfield, Phys. Rev. Lett. **56**, 1007 (1986).
[33] R. Blümel and U. Similansky, J. Opt. Soc. Am. **7**, 664 (1990).
[34] E. J. Heller, Phys. Rev. Lett. **53**, 1515 (1984).
[35] D. Wintgen and A. Honig, Phys. Rev. Lett. **63**, 146 (1989).